LETTER

doi:10.1038/nature21051

Arrays of horizontal carbon nanotubes of controlled chirality grown using designed catalysts

Shuchen Zhang[1]*, Lixing Kang[1,2]*, Xiao Wang[3,4], Lianming Tong[1], Liangwei Yang[1], Zequn Wang[1], Kuo Qi[5], Shibin Deng[1], Qingwen Li[2], Xuedong Bai[5], Feng Ding[3,4,6] & Jin Zhang[1]

The semiconductor industry is increasingly of the view that Moore's law—which predicts the biennial doubling of the number of transistors per microprocessor chip—is nearing its end[1]. Consequently, the pursuit of alternative semiconducting materials for nanoelectronic devices, including single-walled carbon nanotubes (SWNTs), continues[2–4]. Arrays of horizontal nanotubes are particularly appealing for technological applications because they optimize current output. However, the direct growth of horizontal SWNT arrays with controlled chirality, that would enable the arrays to be adapted for a wider range of applications and ensure the uniformity of the fabricated devices, has not yet been achieved. Here we show that horizontal SWNT arrays with predicted chirality can be grown from the surfaces of solid carbide catalysts by controlling the symmetries of the active catalyst surface. We obtained horizontally aligned metallic SWNT arrays with an average density of more than 20 tubes per micrometre in which 90 per cent of the tubes had chiral indices of (12, 6), and semiconducting SWNT arrays with an average density of more than 10 tubes per micrometre in which 80 per cent of the nanotubes had chiral indices of (8, 4). The nanotubes were grown using uniform size Mo_2C and WC solid catalysts. Thermodynamically, the SWNT was selectively nucleated by matching its structural symmetry and diameter with those of the catalyst. We grew nanotubes with chiral indices of ($2m$, m) (where m is a positive integer), the yield of which could be increased by raising the concentration of carbon to maximize the kinetic growth rate in the chemical vapour deposition process. Compared to previously reported methods, such as cloning[5,6], seeding[7,8] and specific-structure-matching growth[9–11], our strategy of controlling the thermodynamics and kinetics offers more degrees of freedom, enabling the chirality of as-grown SWNTs in an array to be tuned, and can also be used to predict the growth conditions required to achieve the desired chiralities.

The growth of SWNTs can be thermodynamically and kinetically controlled[12,13]. Thermodynamic control is affected by the nature of the catalysts used (including their composition and state) and by the interfacial energies between the catalysts and the SWNTs[12]. On the other hand, external factors such as temperature[14,15] and the gas environment[16] influence the kinetic growth rate of SWNTs. Thermodynamics determines the initial species of carbon nanotube, depending on the interfacial energy between the nanotube and the catalyst. As shown in Fig. 1, for solid catalysts, crystal symmetry should be taken into account instead of structure matching when considering the stable existence of carbon nanotubes. Symmetry, which is often used in crystal growth, can be introduced to realize the growth of carbon nanotubes because they can be thought of as a crystal of carbon. Therefore, perfect symmetry matching leads to low formation energies and then high populations of carbon nanotubes with symmetries similar to those of the catalysts, and carbon nanotubes with high symmetry are more commonly observed and may potentially be enriched. On the other hand, during the growth process of carbon nanotubes, kinetic growth rates determine the lengths of the tubes. A slower growth rate shortens the lifetime of the catalysts because too much carbon concentrates on the surfaces of the catalysts; consequently, nanotubes with shorter lengths are attained. For kinetics-favoured growth and when enough carbon fragments are present, theory[12] shows that the nanotubes with the most geometry-imposed kinks (with a chiral angle of 19.1°) will grow with the fastest rate for a given diameter d. Kinetic growth is also governed by the concentration of the carbon source. Of the species of carbon

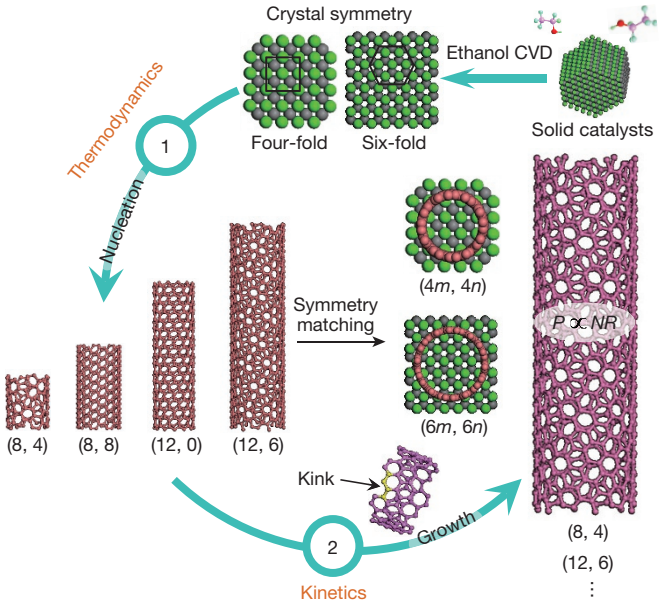

Figure 1 | Two-step control of the chirality of SWNTs in ethanol chemical vapour deposition (CVD). (1) Symmetry matching between the nanotubes and solid catalysts leads to selective nucleation in thermodynamics. The nucleation probability of a certain chiral carbon nanotube N is related to its formation energy on the catalyst ΔE_s: $N \propto \exp[-\Delta E_s/(kT)]$, where k is the Boltzmann constant and T is temperature. (2) During the growth process of SWNTs, the kinetic growth rate R is related to the number of kinks χ_{kinks}: $R \propto \chi_{kinks}$. The ($2m$, m) carbon nanotubes have the fastest growth rate. By combining the thermodynamics (N) and kinetics (R), predictable ($2m$, m) carbon nanotubes with high symmetry can be enriched, with their population (P) described by $P \propto NR$. More specifically, the tubes have chiralities of ($4m$, $4n$) and ($6m$, $6n$), where $m = 2n$ and $n = 1, 2, 3\ldots$. The green and grey spheres represent tungsten and carbon atoms, respectively.

[1]Center for Nanochemistry, Beijing Science and Engineering Center for Nanocarbons, Beijing National Laboratory for Molecular Sciences, Key Laboratory for the Physics and Chemistry of Nanodevices, College of Chemistry and Molecular Engineering, Peking University, Beijing 100871, China. [2]Suzhou Institute of Nanotech and Nanobionics, Chinese Academy of Sciences, Suzhou 215123, China. [3]Center for Multidimensional Carbon Materials, Institute for Basic Science, Ulsan 689-798, South Korea. [4]Institute of Textiles and Clothing, Hong Kong Polytechnic University, Hong Kong, China. [5]Institute of Physics, Chinese Academy of Sciences, Beijing 100190, China. [6]School of Materials Science and Engineering, Ulsan National Institute of Science and Technology, Ulsan 689-798, South Korea.
*These authors contributed equally to this work.

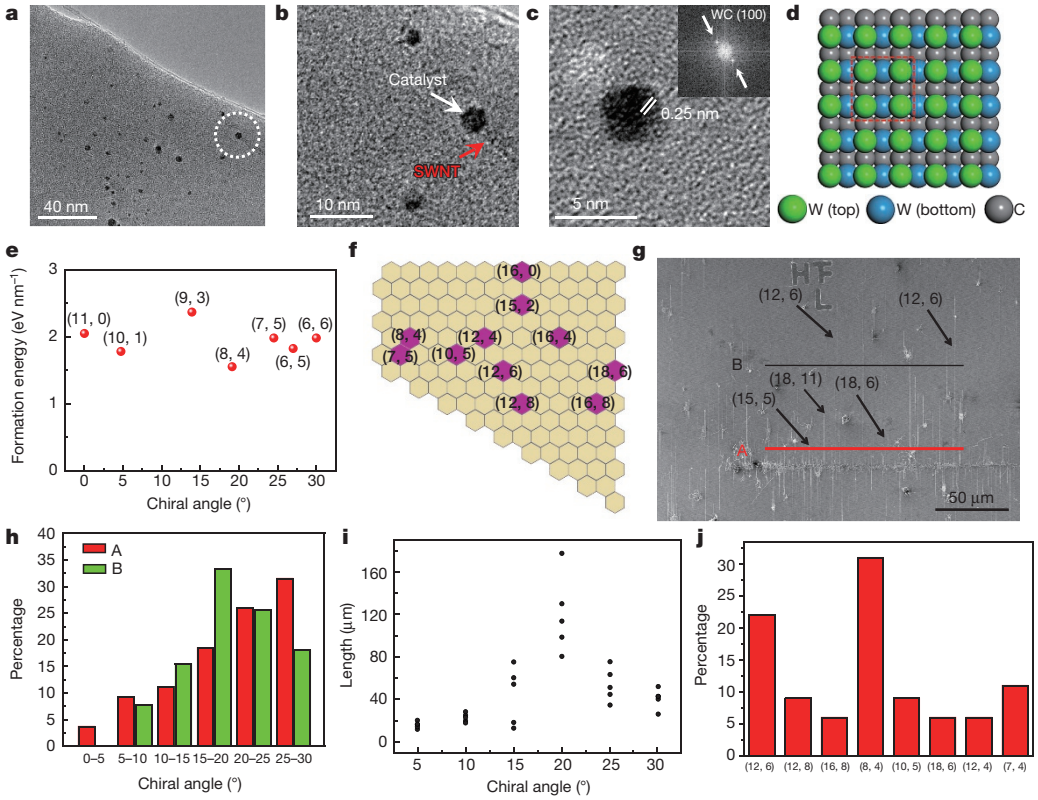

Figure 2 | The effects of symmetry matching and kinetic growth on the distribution of the chirality of SWNTs. a, TEM image of an individual suspended SWNT (indicated by the white dashed circle) with a catalyst on Si_3N_4 film with a thickness of 20 nm. **b**, A close-up of the TEM image in **a** showing the alignment between the SWNT and catalyst. **c**, HRTEM image of the catalyst and corresponding fast Fourier transform of the WC nanoparticle in **b**. Spots corresponding to the (100) planes are indicated using arrows. The image shows that the axis of the SWNT is perpendicular to the (100) fringes of the WC nanoparticles. The spacing between the (100) planes of the WC catalyst is 0.25 nm. **d**, The atomic model of the (100) plane of the WC catalyst, demonstrating quasi-four-fold symmetry. **e**, Density functional theory calculations of the formation energies of tubes with similar diameter on the (100) plane of the WC catalyst demonstrates that the (8, 4) tubes match well with the (100) plane of the WC catalyst in the symmetry. **f**, Many tubes with four-fold symmetry (pink hexagons) were found on WC catalysts (cream background) in experiments. **g**, **h**, With the abrupt increase in the ratio of carbon source during the growth on quartz substrate, the SWNTs at the back (A, total of 65 tubes) and front (B, total of 58 tubes) of the catalyst zone can be recognized by their optical spectra, and have different distributions of (n, m). The (12, 6) tubes are the longest of all the SWNTs. **i**, For some of the SWNTs detected in **g** (those for which the chirality could be determined), the nanotubes with chiral angles closer to 19.1° are much longer than the others. **j**, For WC catalysts, owing to the thermodynamics and kinetics, the tubes with high symmetry and a chiral angle of 19.1° make up a large percentage of the 345 tubes that were detected in the Raman spectra.

nanotubes set by four- and six-fold symmetry, the (8, 4), (12, 6) and other (2m, m) carbon nanotubes (which have a chiral angle of 19.1°) are obtained in the highest populations P, given by $P \propto NR$, where N is nucleation probability of a certain chiral type and R is the kinetic growth rate. This result indicates that it should be possible to enrich SWNTs with specific chirality (corresponding to a chiral angle of 19.1°) and four- or six-fold symmetry by controlling their diameters.

Experimental data and calculations (Fig. 2) confirm the symmetry matching in thermodynamics- and kinetics-promoted growth. As seen using transmission electron microscopy (TEM), a tube was grown directly on the Si_3N_4 grid using tungsten carbide (WC) catalysts (Fig. 2a). Along this tube, a WC catalyst was found at its end (Fig. 2b). High-resolution TEM (HRTEM; Fig. 2c) shows the exact structure of the catalyst, with 0.25-nm spacing between the (100) planes, and the corresponding fast Fourier transform pattern verifies that the (100) plane is perpendicular to the axis of the carbon nanotube. This pattern confirms that the tube grew along the (100) plane of the WC solid catalyst, as shown in Fig. 2c. Figure 2d displays an atomic model of the (100) plane of the WC catalyst, showing the quasi-four-fold symmetry. Carbon nanotubes, as a solid crystal of carbon, will grow from catalysts while obeying the crystal growth rule, which requires symmetry matching. Zigzag, armchair and chiral carbon nanotubes with similar diameters and different symmetries are considered in Fig. 2e. A detailed calculation (see Extended Data Fig. 1 and Supplementary Information) shows that the tubes that have the same symmetry as the catalysts, such as (8, 0), (12, 0) and (8, 4) tubes, have lower formation energies compared with the others. The (8, 4) tubes have the lowest formation energy of those with similar diameters. In experiments, (8, 4), (12, 8), (12, 4), (16, 0), (16, 8) and other four-fold-symmetric tubes were obtained in the largest numbers (Fig. 2f).

As well as thermodynamics, kinetics is another important factor that affects the growth of carbon nanotubes. In theory, kinetic control is related to the number of kinks in the tubes, as reported previously[12] and discussed above. (2m, m) carbon nanotubes, which have 19.1° chirality, were usually kinetically favoured because they have the most kinks. As further confirmation of the role of kinetic control, the ratio of C/H (initially 100/200) abruptly increased after 5 min of growth to 100/0. The tubes were distinguished by their optical absorption spectra; the results are shown in Fig. 2g. We found that more (12, 6) tubes appeared at locations far away from the catalyst zone, and that the SWNTs with chiral angles closer to 19.1° were much longer, indicating the favoured growth of (12, 6) SWNTs with the increased carbon feedstock. The statistics shown in Fig. 2h indicate that, near the catalyst zone, the tubes with bigger chiral angles are more prevalent, consistent with previous reports[13], whereas far away from the catalyst zone the chiral angles of the most commonly observed tubes are about 19.1°. Fig. 2i verifies

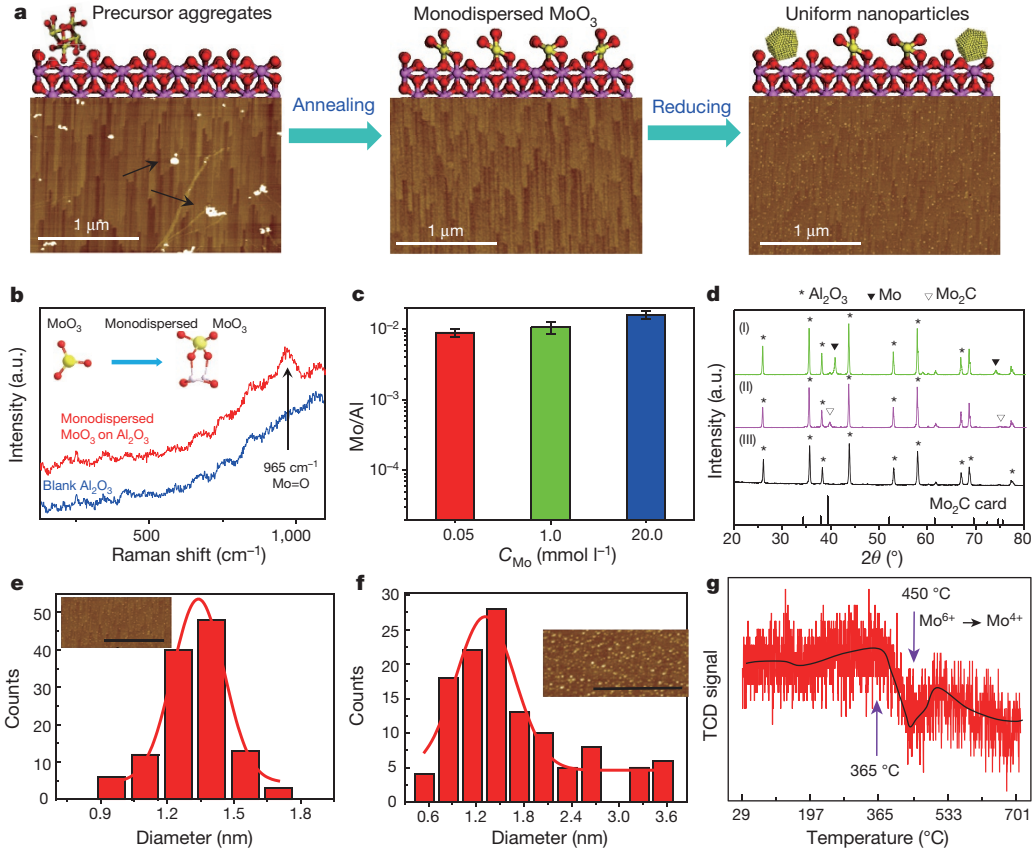

Figure 3 | Formation of uniform catalysts using a monodispersed process. a, Schematic of the process used to obtain monodispersed MoO_3 through annealing on a sapphire substrate (top). The corresponding AFM images are also shown (bottom). **b**, Raman spectrum showing that MoO_3 was monodispersed on the Al_2O_3 support. The peak at 965 cm^{-1} represents the vibration of Mo=O. a.u., arbitrary units. **c**, The average atomic ratio of Mo and Al over three replicates obtained using XPS with different amounts of precursor loaded on the sapphire substrate; C_{Mo} is the concentration of Mo in the solution. The standard deviations of the Mo/Al ratio (shown as error bars) are 1.20×10^{-3}, 2.05×10^{-3} and 2.11×10^{-3} for $C_{Mo} = 0.05$ mmol l^{-1}, $C_{Mo} = 1.0$ mmol l^{-1} and $C_{Mo} = 20$ mmol l^{-1}, respectively. **d**, XRD patterns showing the transformation from monodispersed MoO_3 to Mo_2C catalysts during the growth process. (I), (II) and (III) represent, the reduced Mo nanoparticles, Mo_2C catalysts after introducing a carbon source, and MoO_3 monodispersed on an Al_2O_3 support respectively. The bottom row is the standard Mo_2C card. **e**, **f**, Size distributions (bars) and Gaussian fits (red lines) of the catalyst nanoparticles after reduction at initial temperatures of 450 °C (**e**; mean, 1.36 nm; standard deviation, 0.23 nm) and 800 °C (**f**; mean, 1.59 nm; standard deviation, 0.65 nm). The insets show the corresponding AFM images; scale bars, 1 μm. **g**, H_2-TPR profile of monodispersed MoO_3 on an Al_2O_3 support, showing the slow transformation from Mo^{6+} to Mo^{4+} starting at 365 °C; the best transformation temperature is 450 °C. The red line is the true signal we obtained and the black line is a fit line. TCD, thermal conductivity detector.

that the tubes have the greatest length when their chiral angle is near 19.1°. The shorter tubes had lengths similar to those of the tubes measured after only 5 min of growth (see Extended Data Fig. 2). The kinetic control governed by the growth condition is also demonstrated in Extended Data Fig. 3. These results show that kinetic growth could maintain the activity of the catalysts by relieving the aggregation of excessive carbon on catalysts. Moreover, when hydrogen was used in the growth process, the kinetic growth rate was weakened by the etching effect of hydrogen. As a result, other SWNTs with similar diameters to ($2m$, m) tubes, but with different chiral angles, appeared and could be detected by Raman spectroscopy (Supplementary Fig. 11), and the percentage of the ($2m$, m) nanotubes was reduced. The kinetic growth control was also applied to other catalysts, including TiO_2, Cr_2O_3 and ZnO (ref. 17), and it was found that the enrichment of (12, 6) SWNTs could also be achieved in these cases (Supplementary Fig. 12). In summary, thermodynamics and kinetics have been combined to control the chirality of carbon nanotubes. When WC catalysts were used, as described in Fig. 2j, symmetry matching led to the growth of nanotubes with four-fold symmetry, such as (8, 4), (12, 4), (12, 8) and (16, 8) tubes, with kinetics enhancing the growth of (8, 4), (10, 5), (12, 6) and (16, 8) tubes. The (10, 5) nanotubes were rarely observed in our experiment, possibly owing to their five-fold symmetry, which is mismatched to the crystal symmetry of catalysts. In fact, (10, 5) SWNTs have rarely been reported in conventional chemical vapour deposition processing[18]. The result of using WC catalysts together with kinetic control is greater numbers of (8, 4) tubes.

Size uniformity of the catalyst nanoparticles is one of the key prerequisites for the growth of the carbon nanotubes with specific chirality, and so can be used to further control the distribution of the tubes. Figure 3a illustrates the route of our strategy to this end. First, $(NH_4)_6Mo_7O_{24}{\bullet}4H_2O$ aggregates were dispersed on a sapphire substrate. The size of the aggregates was typically tens of nanometres. Interestingly, after an annealing process at 1,100 °C, the aggregates disappeared. X-ray photoelectron spectroscopy (XPS; Supplementary Fig. 7) confirmed the existence of molybdenum (Mo) in an oxidized form on the surface of the sample after annealing. As reported elsewhere[19,20], MoO_3 tends to form a monolayer on Al_2O_3, owing to the formation of an Mo–O–Al bond that shares an oxygen atom with Al, and the excess MoO_3 vaporizes as a result of its high volatility. Raman spectroscopic measurements show that the peak position of the Mo=O bond shifted from 998 cm^{-1} to 965 cm^{-1} (Fig. 3b), confirming the formation of monodispersed MoO_3 on the sapphire substrate after annealing[21,22]. XPS characterization also showed that the atomic ratio Mo/Al on the surface stayed almost constant despite the different

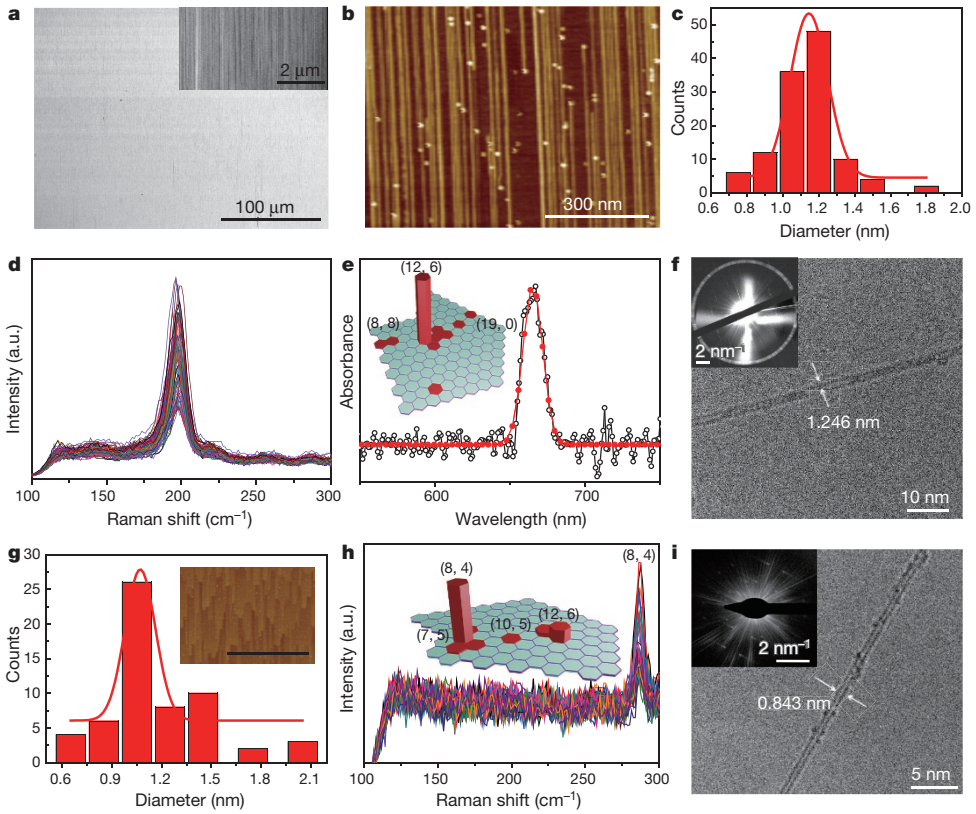

Figure 4 | Successful growth of (12, 6) and (8, 4) SWNTs arrays using uniform catalysts, and their characterizations. **a**, SEM image of the as-grown (12, 6) SWNT arrays using Mo_2C catalysts. Inset, a magnified image. **b**, **c**, The corresponding AFM image (**b**) and size distribution and Gaussian fit of the (12, 6) SWNT array (**c**; mean, 1.21 nm; standard deviation, 0.26 nm). **d**, Raman spectra in the RBM region, obtained using line mapping with a scanning step of 1 μm and an excitation of 633 nm. **e**, Ultraviolet–visible–near-infrared absorption spectrum (background-subtracted; open circles) of an aqueous dispersion of SWNTs collected from 40 samples, and the fitted spectrum (red line). Inset, the relative abundances of the various chiralities. **f**, TEM image of carbon nanotubes. Inset, a typical electron diffraction pattern of a (12, 6) nanotube. **g**, The size distribution of catalysts using monodispersed tungsten oxide on sapphire (mean, 1.09 nm; standard deviation, 0.46 nm). Inset, the corresponding AFM image; scale bar, 1 μm. **h**, Raman spectra in the RBM region, obtained using line mapping with a scanning step of 1 μm and an excitation of 633 nm. Inset, the population of the chiral species of the tubes. **i**, Typical TEM image of the SWNTs. Inset, the corresponding electron diffraction pattern.

concentrations of $(NH_4)_6Mo_7O_{24}{\bullet}4H_2O$ used (0.05 mmol l^{-1}, 1.0 mmol l^{-1} and 20.0 mmol l^{-1}; see Fig. 3c and Supplementary Fig. 8). X-ray diffraction (XRD) characterization of a parallel bulk sample revealed that MoO_3 disappeared after annealing (Fig. 3d) and was transformed into Mo after a moderate reduction at the starting temperature of 450 °C in hydrogen atmosphere[23]. After reduction, uniformly sized Mo nanoparticles appeared on the sapphire substrate, as depicted in the atomic force microscopy (AFM) image. The Mo nanoparticles were readily transformed into uniform Mo_2C catalysts, which could be used to grow carbon nanotubes[24] once introduced into the carbon source. Note that the reducing temperature is the determining factor driving the uniformity of the catalyst nanoparticles. For MoO_3, a narrow distribution of 1.36 ± 0.23 nm (where the error given here and elsewhere is the standard deviation) can be obtained using a reducing temperature starting at 450 °C (Fig. 3e). However, when the initial temperature was increased to 800 °C, the size distribution became much broader: 1.59 ± 0.65 nm (Fig. 3f). We explored the origin of this difference using hydrogen temperature-programmed reduction (H_2-TPR), a useful characterization technique for investigating chemical information at the surface of substrates. Figure 3g shows the TPR profile of MoO_3 on an Al_2O_3 support, in which a dip appears at 450 °C owing to the reduction from Mo^{6+} to Mo^{4+} under H_2 atmosphere. Mo^{4+} was further reduced to Mo with increasing temperature. This two-step reduction is a slower process than the one-step reduction (from Mo^{6+} to Mo) starting at temperatures higher than 450 °C, and the diffusive migration of Mo is also slower, facilitating the formation of more uniform catalyst nanoparticles.

On the basis of these results, we developed a chiral control method to realize the enrichment of carbon nanotubes with single chirality. We successfully grew (12, 6) SWNT arrays on a sapphire substrate using uniform Mo_2C catalysts. A scanning electron microscopy (SEM) image (Fig. 4a) of the as-grown (12, 6) SWNT array shows that the nanotubes were well aligned over a large scale (hundreds of micrometres), with an average density of more than 20 tubes per micrometre; the inset in Fig. 4a displays a high-magnification SEM image of a randomly selected area. AFM (Fig. 4b and Extended Data Fig. 4) reveals that the highest density of the as-grown, horizontally aligned SWNT arrays was about 40 tubes per micrometre. The tubes had a narrow distribution of diameters, centred at approximately 1.21 nm (Fig. 4c)—very similar to the diameter of the (12, 6) tubes. Raman measurements (Fig. 4d) show that the radial breathing mode (RBM) peaks were mainly concentrated at about 197 cm^{-1} using 633-nm laser excitation, and the Breit–Wigner–Fano line shape of the corresponding tangential mode (G mode; a characteristic feature of metallic nanotubes; see Supplementary Fig. 1 and Fig. 2) is clearly seen. From the RBM peak position, the tube diameter is estimated to be 1.26 nm, consistent with our AFM measurements. According to the Kataura plot[25], the chirality of the as-grown SWNTs was assigned to be (12, 6). The abundance of (12, 6) nanotubes in the SWNT array was estimated to be greater than 90%, using several methods. Raman line mapping measurements with different excitation lasers (488 nm, 514 nm, 633 nm and 785 nm) at the same area were performed, and the statistics of RBM peaks (Extended Data Fig. 5 and Supplementary Table 2) gives an abundance of about 92% among all of the detected SWNTs. To achieve a more accurate measure, SWNTs collected from more than 40 arrays were dispersed in a sodium dodecyl sulfate solution[26,27] for ultraviolet–visible–near-infrared absorption spectral characterization (Fig. 4e). The abundance of (12, 6) SWNTs was estimated to be higher than 90%. In addition, we also correlated AFM and Raman measurements of the same sample. The tube-by-tube counting of individual SWNTs also showed that the percentage of (12, 6) tubes was more than 90%. Five randomly selected sets of parallel experiments are presented in Supplementary Table 6, showing that the worst selectivity for (12, 6) tubes is about 84% and the best is 92%. The assignment was further verified by electron diffraction characterization on isolated SWNTs transferred to a copper grid (Fig. 4f and Extended Data Fig. 6). The HRTEM gives a tube diameter of 1.246 nm. The optical reflection spectrum (Supplementary Fig. 3) of the nanotube array transferred to a SiO_2 (90 nm)/Si substrate confirms the enrichment of (12, 6) SWNTs. Extended Data Fig. 7 shows that the ratio of the intensities of the G and D peaks

(G/D; indicating perfection of the carbon nanotubes and defects in the carbon nanotubes, respectively) is about 22, which verifies the high quality of the tubes.

The enrichment of semiconducting nanotubes of defined chirality is crucial for achieving high-performance SWNT-based nanoelectronic devices. Using our strategy for the growth of carbon nanotubes, we successfully enriched semiconducting (8, 4) SWNTs with an abundance of about 80% in an array on a sapphire substrate using uniform WC catalysts. In this process, WO_3 (ref. 28) was used as precursor, owing to its tendency to form smaller catalysts than does MoO_3. Figure 4g shows that the size of the catalyst nanoparticles after reduction is 1.09 ± 0.46 nm. The SEM image of the as-grown SWNT array is shown in Extended Data Fig. 8a. The density of the nanotubes was estimated to be greater than 10 tubes per micrometre. The statistics in Extended Data Fig. 8b show that the mean diameter of the SWNTs was 0.87 ± 0.17 nm. Raman spectra (Fig. 4h) demonstrates that the RBM peaks were concentrated at approximately 283 cm^{-1}, corresponding to (8, 4) SWNTs[29]. The chirality assignment was further confirmed by the optical reflection spectrum (Extended Data Fig. 9 and Supplementary Fig. 4) and electron diffraction (Fig. 4i), and the abundance was estimated to be about 80% (Supplementary Table 4), which is close to the population calculated in Supplementary Fig. 24 and Supplementary Table 7. To the best of our knowledge, this is the highest purity of single-chirality semiconducting SWNTs in a horizontal array reported so far[18,30]. The electrical properties of the two arrays—(12, 6) and (8, 4) tubes—are compared in Extended Data Fig. 10.

Our findings demonstrate that selective nucleation of carbon nanotubes from symmetry matching between catalysts and nanotubes and the growth kinetics of SWNTs in a hydrogen-free atmosphere favours the enrichment of SWNTs with chiral angles of 19.1°. We grew arrays of (12, 6) and (8, 4) nanotubes with chiral purities of greater than 90% and 80%, and surface densities of more than 20 and 10 tubes per micrometre, respectively. By optimizing the size selectivity, such as the size of the catalyst and the reducing temperature, the purity of ($2m$, m) nanotubes with high symmetry can be increased, and we anticipate that such SWNT arrays of high density, particularly the semiconducting ($2m$, m) SWNTs, can be readily developed for future nanoelectronic device applications.

Online Content Methods, along with any additional Extended Data display items and Source Data, are available in the online version of the paper; references unique to these sections appear only in the online paper.

Data Availability All data supporting the findings of this study are available within the paper and its Supplementary Information. The data relating to Figs 2–4 and Extended Data Figs 1, 3, 7–10 are provided as Source Data.

Received 22 February; accepted 7 December 2016.
Published online 15 February 2017.

1. Waldrop, M. M. The chips are down for Moore's law. *Nature* **530,** 144–147 (2016).
2. Cao, Q. *et al.* End-bonded contacts for carbon nanotube transistors with low, size-independent resistance. *Science* **350,** 68–72 (2015).
3. Shulaker, M. M. *et al.* Carbon nanotube computer. *Nature* **501,** 526–530 (2013).
4. Franklin, A. D. The road to carbon nanotubes transistors. *Nature* **498,** 443–444 (2013).
5. Yao, Y. G., Feng, C. Q., Zhang, J. & Liu, Z. F. "Cloning" of single-walled carbon nanotubes via open-end growth mechanism. *Nano Lett.* **9,** 1673–1677 (2009).
6. Liu, J. *et al.* Chirality-controlled synthesis of single-wall carbon nanotubes using vapour-phase epitaxy. *Nat. Commun.* **3,** 1199 (2012).
7. Sanchez-Valencia, J. R. *et al.* Controlled synthesis of single-chirality carbon nanotubes. *Nature* **512,** 61–64 (2014).
8. Yu, X. *et al.* Cap formation engineering: from opened C_{60} to single-walled carbon nanotubes. *Nano Lett.* **10,** 3343–3349 (2010).
9. Yang, F. *et al.* Chirality-specific growth of single-walled carbon nanotubes on solid alloy catalysts. *Nature* **510,** 522–524 (2014).
10. He, M. *et al.* Chiral-selective growth of single-walled carbon nanotubes on lattice-mismatched epitaxial cobalt nanoparticles. *Sci. Rep.* **3,** 1460 (2013).
11. Zhu, H., Suenaga, K., Wei, J., Wang, K. & Wu, D. A strategy to control the chirality of single-walled carbon nanotubes. *J. Cryst. Growth* **310,** 5473–5476 (2008).
12. Artyukhov, V. I., Penev, E. S. & Yakobson, B. I. Why nanotubes grow chiral. *Nat. Commun.* **5,** 4892 (2014).
13. Ding, F., Harutyunyan, A. R. & Yakobson, B. I. Dislocation theory of chirality-controlled nanotube growth. *Proc. Natl Acad. Sci. USA* **106,** 2506–2509 (2009).
14. Liu, B., Ren, W., Li, S., Liu, C. & Cheng, H. M. High temperature selective growth of single-walled carbon nanotubes with a narrow chirality distribution from a CoPt bimetallic catalyst. *Chem. Commun.* **48,** 2409–2411 (2012).
15. Yao, Y. *et al.* Temperature-mediated growth of single-walled carbon-nanotube intramolecular junctions. *Nat. Mater.* **6,** 283–286 (2007).
16. He, M., Jiang, H., Kauppinen, E. I. & Lehtonen, J. Diameter and chiral angle distribution dependencies on the carbon precursors in surface-grown single-walled carbon nanotubes. *Nanoscale* **4,** 7394–7398 (2012).
17. Huang, S., Cai, Q., Chen, J., Qian, Y. & Zhang, L. Metal-catalyst-free growth of single-walled carbon nanotubes on substrates. *J. Am. Chem. Soc.* **131,** 2094–2095 (2009).
18. Bachilo, S. M. *et al.* Narrow (n, m)-distribution of single-walled carbon nanotubes grown using a solid supported catalyst. *J. Am. Chem. Soc.* **125,** 11186–11187 (2003).
19. Xie, Y.-C. & Tang, Y.-Q. Spontaneous monolayer dispersion of oxides and salts onto surfaces of supports: applications to heterogeneous catalysis. *Adv. Catal.* **37,** 1–43 (1990).
20. Chen, Y. & Zhang, L. Surface interaction model of γ-alumina-supported metal oxides. *Catal. Lett.* **12,** 51–62 (1992).
21. Gao, J. *et al.* Identification of molybdenum oxide nanostructures on zeolites for natural gas conversion. *Science* **348,** 686–690 (2015).
22. Hu, H., Wachs, I. E. & Bare, S. R. Surface structures of supported molybdenum oxide catalysts: characterization by Raman and Mo L_3-Edge XANES. *J. Phys. Chem.* **99,** 10897–10910 (1995).
23. Fenglan, Z. *et al.* Characterization of molybdenum oxide supported on α-Al_2O_3. *J. Mater. Chem.* **13,** 1206–1209 (2003).
24. Zhang, S., Tong, L., Hu, Y., Kang, L. & Zhang, J. Diameter-specific growth of semiconducting SWNT arrays using uniform Mo_2C solid catalyst. *J. Am. Chem. Soc.* **137,** 8904–8907 (2015).
25. Dresselhaus, M. S., Dresselhaus, G., Saito, R. & Jorio, A. Raman spectroscopy of carbon nanotubes. *Phys. Rep.* **409,** 47–99 (2005).
26. Hu, Y., Chen, Y., Li, P. & Zhang, J. Sorting out semiconducting single-walled carbon nanotube arrays by washing off metallic tubes using SDS aqueous solution. *Small* **9,** 1306–1311 (2013).
27. Tanaka, T., Jin, H., Miyata, Y. & Kataura, H. High-yield separation of metallic and semiconducting single-wall carbon nanotubes by agarose gel electrophoresis. *Appl. Phys. Express* **1,** 114001 (2008).
28. Gutiérrez-Alejandre, A., Ramírez, J. & Busca, G. The electronic structure of oxide-supported tungsten oxide catalysts as studied by UV spectroscopy. *Catal. Lett.* **56,** 29–33 (1998).
29. Bachilo, S. M. *et al.* Structure-assigned optical spectra of single-walled carbon nanotubes. *Science* **298,** 2361–2366 (2002).
30. Wang, H. *et al.* Catalysts for chirality selective synthesis of single-walled carbon nanotubes. *Carbon* **81,** 1–19 (2015).

Supplementary Information is available in the online version of the paper.

Acknowledgements We are grateful to K. Jiang (Tsinghua University, China), K. Liu (Peking University, China) and R. Horn (Deakin University, Australia) for discussions. This work was supported by the Ministry of Science and Technology of China (2016YFA0200101 and 2016YFA0200104) and the National Natural Science Foundation of China (grant 51432002, 21129001 and 21233001).

Author Contributions J.Z., S.Z., L.K. and F.D. conceived and designed the experiments. S.Z., L.K., X.W., L.Y. and Z.W. performed the experiments. K.Q. and X.B. were responsible for technical assistance with the electron diffraction pattern of carbon nanotubes using HRTEM. J.Z., S.Z., L.K., L.T., F. D. and X.W. performed the data analysis. J.Z., S.Z. and L.T. wrote the manuscript. All authors discussed the results and commented on the manuscript.

Author Information Reprints and permissions information is available at www.nature.com/reprints. The authors declare no competing financial interests. Readers are welcome to comment on the online version of the paper. Correspondence and requests for materials should be addressed to J.Z. (jinzhang@pku.edu.cn).

Reviewer Information *Nature* thanks A. Harutyunyan and the other anonymous reviewer(s) for their contribution to the peer review of this work.

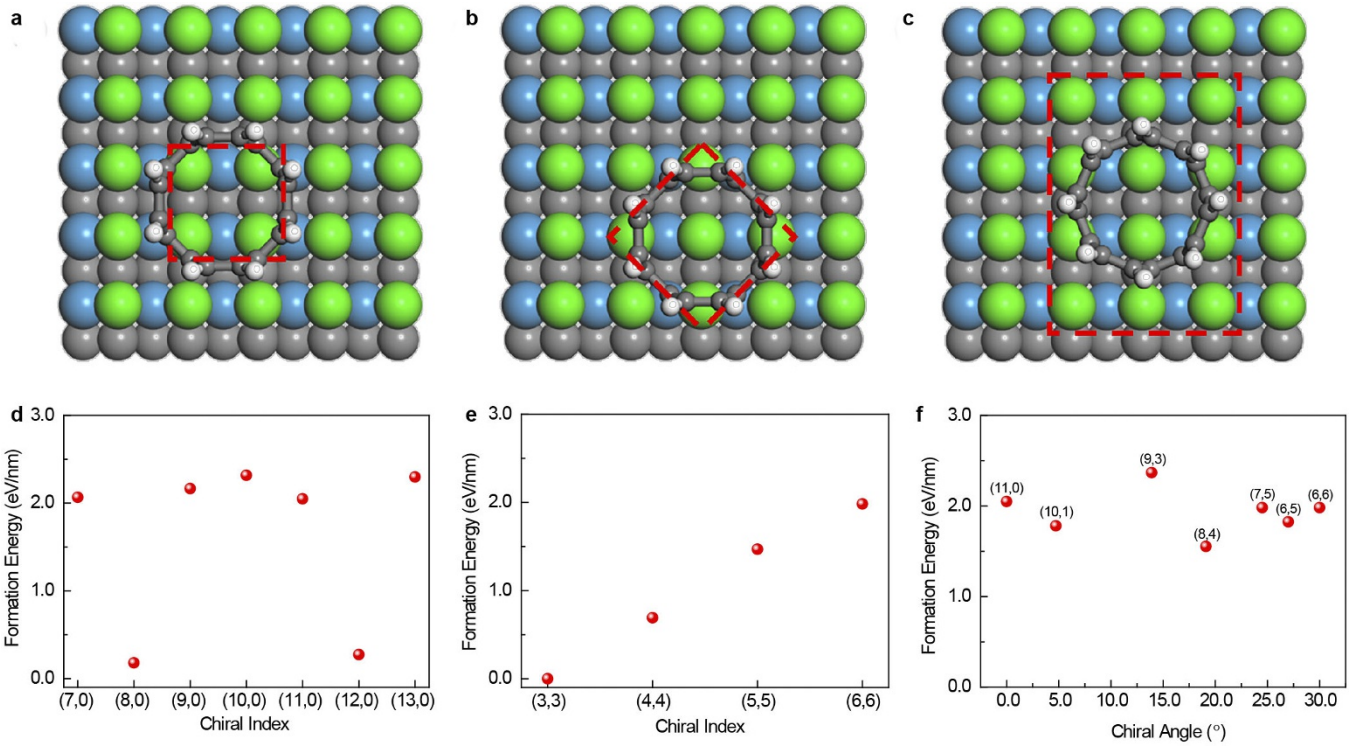

Extended Data Figure 1 | Models and theoretical calculations on the symmetry matching between catalysts and carbon nanotubes. a–c, The high-symmetry relative position of SWNT on WC (100) surface: square (**a**), diamond (**b**) and rectangle (**c**). The relative positions are indicated by red dashed lines. The tungsten and carbon atoms are coloured blue and grey, respectively. The top layer consists of tungsten atoms, and is highlighted in green. **d–f**, The lowest formation energies of SWNTs with different chiralities on WC (100) surface: zigzag-SWNTs (**d**), armchair-SWNTs (**e**) and SWNTs with similar diameters (**f**).

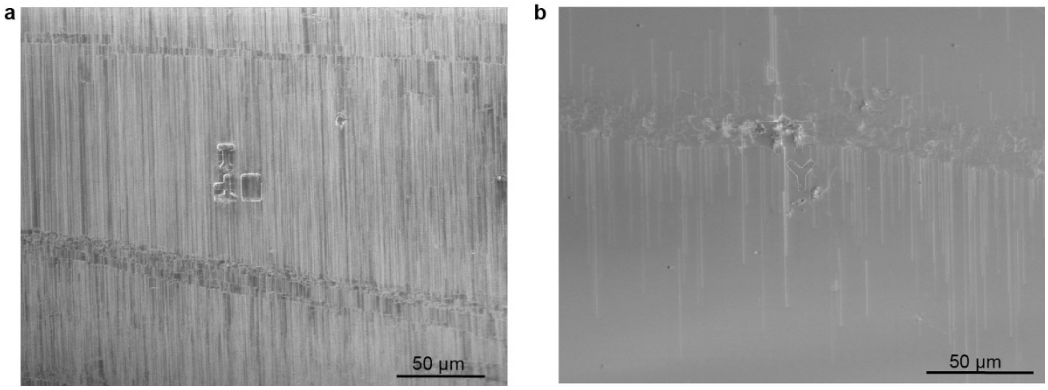

Extended Data Figure 2 | The effect of growth time on the length of tubes. a, **b**, The tubes that were grown for 15 min (**a**) are much longer than those grown for 5 min (**b**). Consequently, we were able to demonstrate kinetically controlled growth following a short period of general growth, as shown in Fig. 2g.

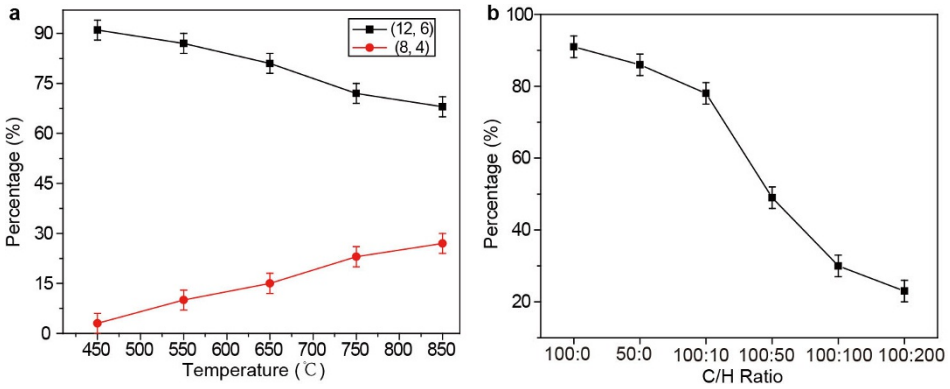

Extended Data Figure 3 | The effects of initial reducing temperature and C/H ratio on the species of tubes. a, The percentages of (12, 6) (black) and (8, 4) (red) SWNTs in (2*m*, *m*) carbon nanotubes grown when using catalysts reduced at different initial temperatures. **b**, The percentage of as-grown (12, 6) nanotubes as a function of C/H ratio during growth at 850 °C when the catalysts were reduced from 450 °C. The error bars show the standard deviations, which are 3%.

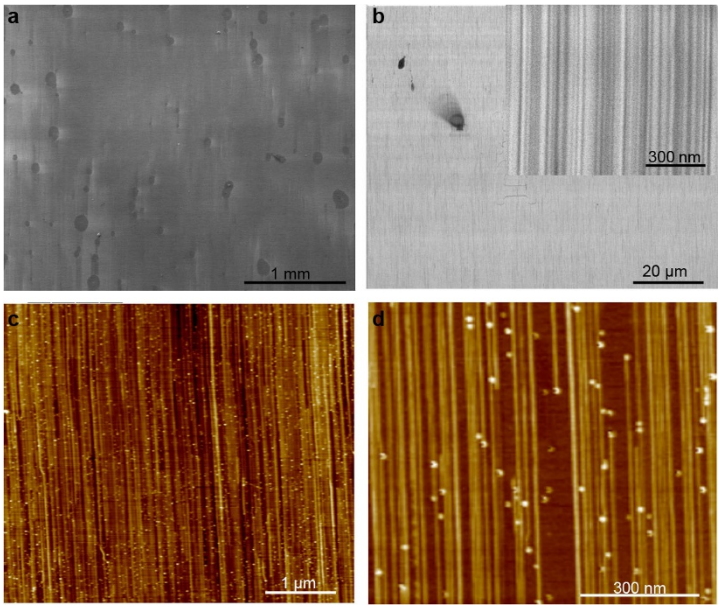

Extended Data Figure 4 | SEM and AFM images of the tubes at different scales. a–**d**, SEM images (**a**, **b**) and AFM images (**c**, **d**) showing the high density of (12, 6) SWNTs in an array grown on the sapphire surface. The average density was about 20 tubes per micrometre, with local densities of more than 40 tubes per micrometre in certain regions (**d** and the inset in **b**).

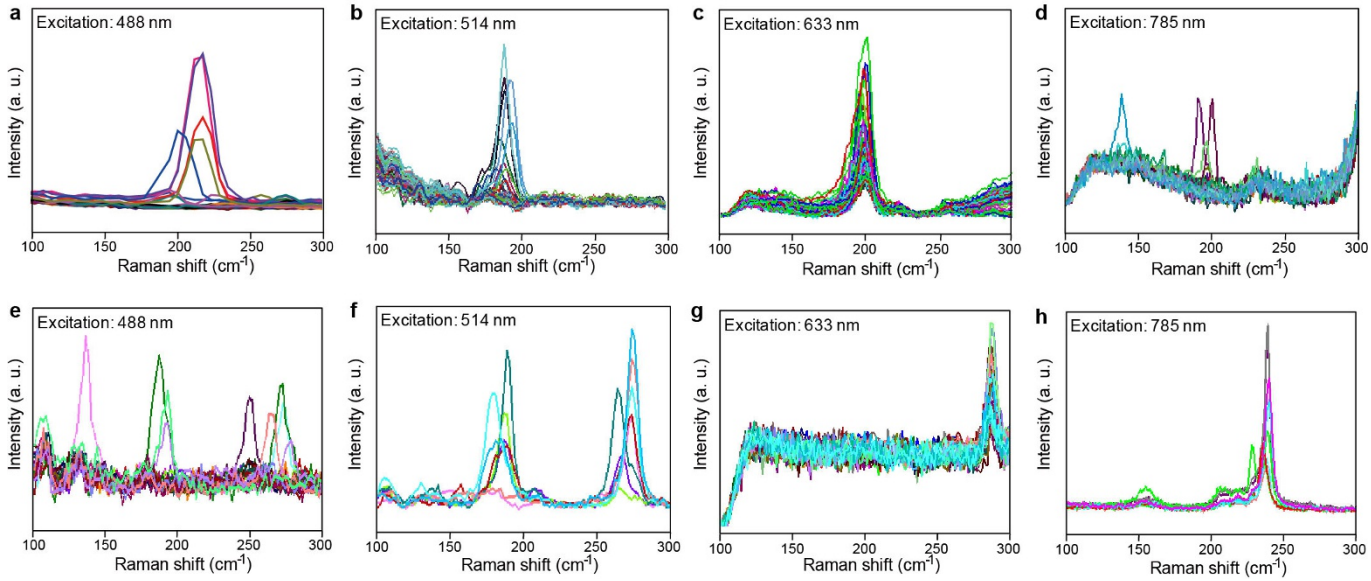

Extended Data Figure 5 | Raman characterizations for (12, 6) and (8, 4) tubes. a–h, Raman spectra of (12, 6) SWNTs using excitation wavelengths of 488 nm (**a**), 514 nm (**b**), 633 nm (**c**) and 785 nm (**d**), and those of (8, 4) SWNTs using excitation wavelengths of 488 nm (**e**), 514 nm (**f**), 633 nm (**g**) and 785 nm (**h**).

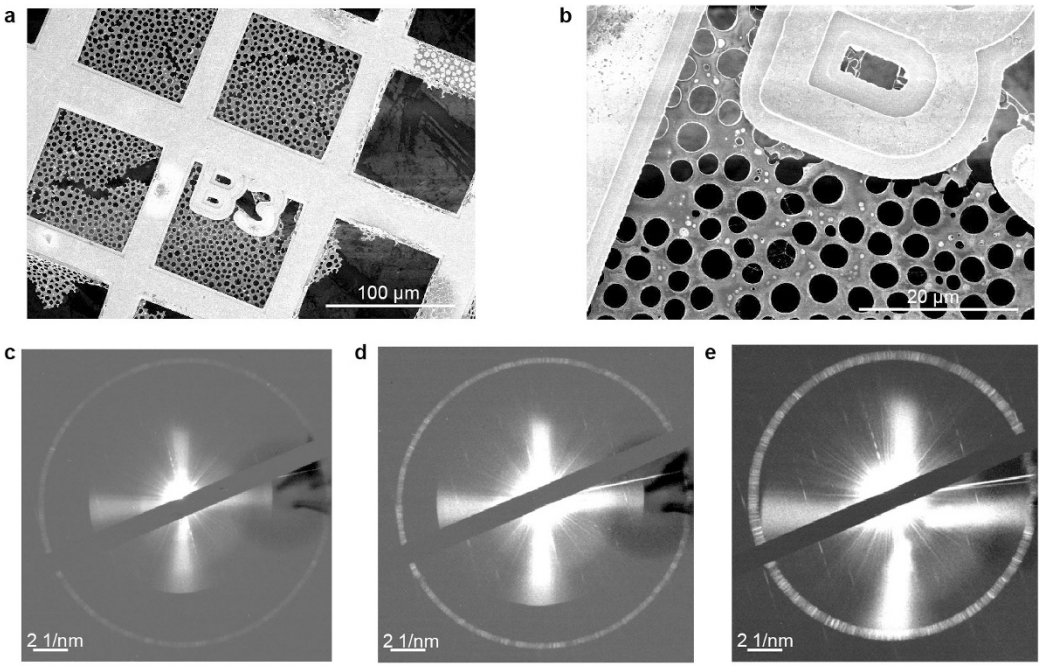

Extended Data Figure 6 | Electron diffraction patterns of (12, 6) tubes on a copper grid. a, **b**, Images of the (12, 6) SWNT array transferred to a copper grid with markers. **c**–**e**, Electron diffraction patterns of the as-grown (12, 6) SWNTs at different places on the different tubes.

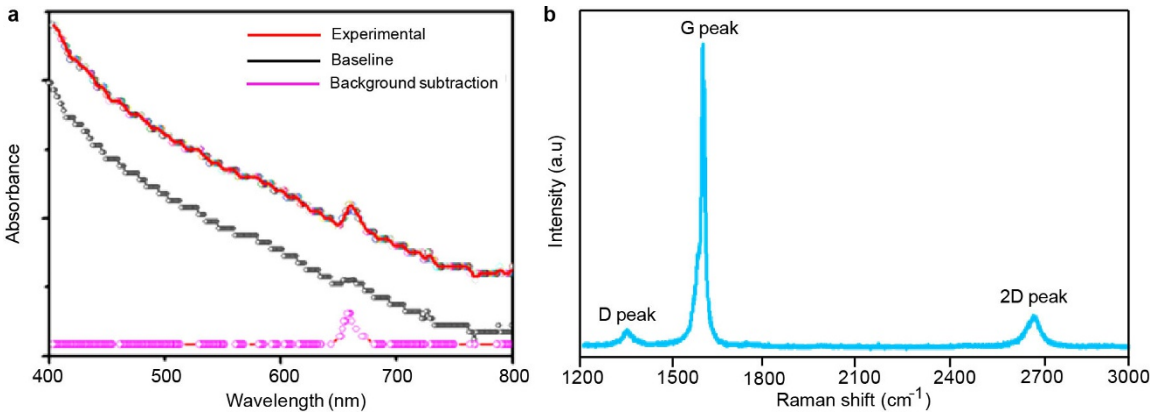

Extended Data Figure 7 | Spectral characterization of (12, 6) tubes. a, **b**, Ultraviolet–visible–near-infrared absorption spectrum of (12, 6) SWNTs (**a**) and their Raman spectrum showing the high quality as indicated by the D peak, G peak and 2D peak (**b**).

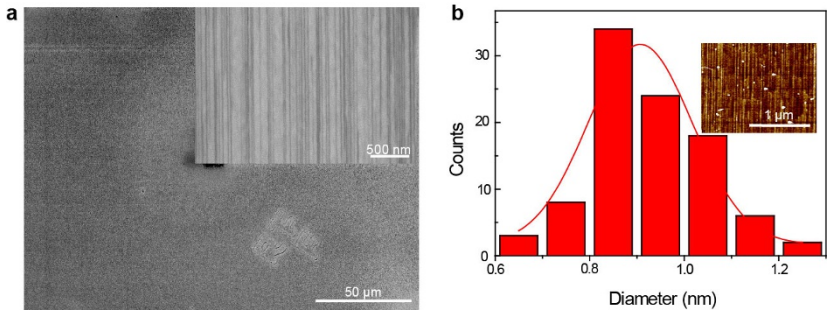

Extended Data Figure 8 | SEM images and the distribution of the diameter of the (8, 4) tubes. a, High density of (8, 4) SWNTs in an array grown on the sapphire surface. **b**, For the (8, 4) array, the average diameter is 0.87 nm, with a standard deviation of 0.17 nm.

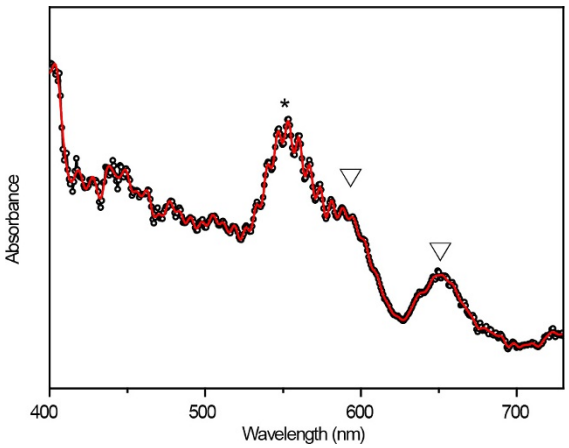

Extended Data Figure 9 | Optical absorption spectrum of the (8, 4) nanotube-enriched arrays on the substrate. There are some (12, 6) tubes in the (8, 4) tubes array. The asterisk represents the (8, 4) tube and the triangles represent the (12, 6) tubes.

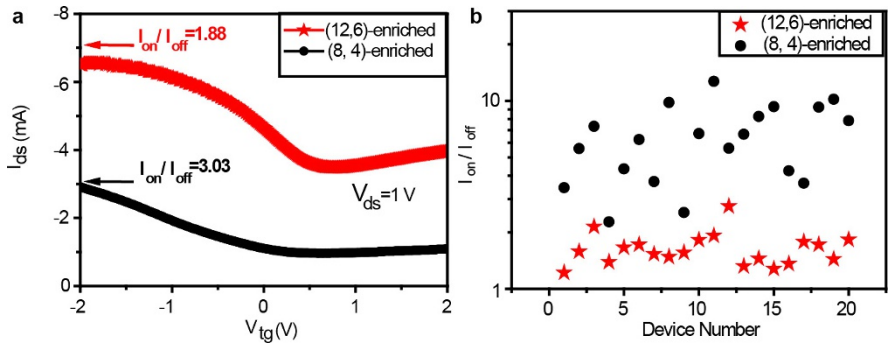

Extended Data Figure 10 | Electrical properties of as-grown carbon nanotube arrays. a, Typical transfer characteristic curves of field-effect transistor devices fabricated on (12, 6)- and (8, 4)-enriched SWNT arrays. **b**, Corresponding statistical results of I_{on}/I_{off} ratios for the two different samples. I_{ds}, drain–source current; I_{on}, maximum I_{ds}; I_{off}, minimum I_{ds}.